Stem Cell Reports
Article

ISSCR

OPEN ACCESS

High Glutathione and Glutathione Peroxidase-2 Levels Mediate Cell-Type-Specific DNA Damage Protection in Human Induced Pluripotent Stem Cells

Benjamin Dannenmann,[1,3] Simon Lehle,[1,3] Dominic G. Hildebrand,[1] Ayline Kübler,[1] Paula Grondona,[1] Vera Schmid,[1] Katharina Holzer,[1] Mirjam Fröschl,[1] Frank Essmann,[1] Oliver Rothfuss,[1] and Klaus Schulze-Osthoff[1,2,*]

[1]Department of Molecular Medicine, Interfaculty Institute for Biochemistry, University of Tübingen, 72076 Tübingen, Germany
[2]German Cancer Consortium (DKTK) and German Cancer Research Center (DKFZ), 69120 Heidelberg, Germany
[3]Co-first author
*Correspondence: kso@uni-tuebingen.de
http://dx.doi.org/10.1016/j.stemcr.2015.04.004

SUMMARY

Pluripotent stem cells must strictly maintain genomic integrity to prevent transmission of mutations. In human induced pluripotent stem cells (iPSCs), we found that genome surveillance is achieved via two ways, namely, a hypersensitivity to apoptosis and a very low accumulation of DNA lesions. The low apoptosis threshold was mediated by constitutive p53 expression and a marked upregulation of proapoptotic p53 target genes of the *BCL-2* family, ensuring the efficient iPSC removal upon genotoxic insults. Intriguingly, despite the elevated apoptosis sensitivity, both mitochondrial and nuclear DNA lesions induced by genotoxins were less frequent in iPSCs compared to fibroblasts. Gene profiling identified that mRNA expression of several antioxidant proteins was considerably upregulated in iPSCs. Knockdown of glutathione peroxidase-2 and depletion of glutathione impaired protection against DNA lesions. Thus, iPSCs ensure genomic integrity through enhanced apoptosis induction and increased antioxidant defense, contributing to protection against DNA damage.

INTRODUCTION

The generation of human induced pluripotent stem cells (iPSCs) from adult somatic cells represents an important advancement in stem cell biology, because of the many potential applications including patient-specific tissue replacement, drug screening, and disease modeling (Okita and Yamanaka, 2011; Robinton and Daley, 2012). In addition, iPSCs derived from patients of diseases caused by known mutations can generate valuable in vitro models for complex disorders, including aging, diabetes, and neurodegeneration. The iPSCs can be generated through forced expression of a set of transcription factors and share with embryonic stem cells (ESCs) the same cardinal features of self-renewal and pluripotency (Takahashi et al., 2007; Yu et al., 2007; Park et al., 2008).

Pluripotent stem cells have the capacity to differentiate into almost any cell type in the adult organism. This pluripotency, however, requires that, unlike differentiated cells, stem cells must be endowed with superior DNA maintenance and repair systems to ensure genomic stability over multiple generations without propagating DNA errors (Liu et al., 2014). The mechanisms required to maintain genomic integrity in response to DNA damage, which could otherwise compromise competency for tissue renewal, are only poorly understood and have been largely investigated in ESCs. Human ESCs and iPSCs, for instance, have an abbreviated cell cycle with a very brief G1 phase, indicating that mechanisms mediating responses to DNA damage may differ from those in somatic cells (Momcilović et al., 2009, 2010; Filion et al., 2009).

Under physiological conditions, reactive oxygen species (ROS) generated as by-product of mitochondrial respiration are the major source of DNA damage (Schieber and Chandel, 2014). DNA lesions in the absence of DNA repair can lead to cell death, genomic instability, and cancer. There are two major ways how ESCs could principally ensure increased genomic integrity. First, mutation frequencies must be suppressed by low levels of DNA damage accumulation and efficient repair systems. Second, ESCs that accumulate mutations or DNA damage must be rapidly eliminated from the stem cell population. Previous studies suggested that mechanisms of genome surveillance, including DNA repair, are indeed superior in ESCs (Saretzki et al., 2008; Maynard et al., 2008). It was shown that murine ESCs possess highly efficient repair mechanisms resulting in a 100-fold lower mutation frequency compared with embryonic fibroblasts (Cervantes et al., 2002). In addition, murine and human ESCs are hypersensitive to several DNA-damaging agents and readily undergo apoptosis (Qin et al., 2007; Roos et al., 2007; Madden et al., 2011; Liu et al., 2013).

Multiple mechanisms have been described that sensitize ESCs to DNA damage-induced apoptosis. First, human ESCs possess unique ROCK-dependent mechanisms in singularized cells that lead to a myosin-mediated form of cell blebbing, which rapidly triggers apoptosis upon cell detachment (Ohgushi et al., 2010). Second, unlike

differentiated cells, certain human ESC lines have been found to express a constitutively pre-activated form of the proapoptotic BCL-2 protein BAX at the Golgi apparatus, which may quickly translocate to the outer mitochondrial membrane and initiate execution of the intrinsic apoptosis pathway upon DNA damage (Dumitru et al., 2012). Notably, the basal level of pre-activated BAX varies among different human ESC lines and, for example, is not detectable in the H1 cell line. Nonetheless, H1 cells show the typical sensitivity to DNA damage, suggesting that additional mechanisms might be involved in priming ESCs for rapid cell death (Liu et al., 2014).

Although the regulation of pluripotency and genomic stability has been mainly studied in ESCs, very little is known regarding the mechanisms controlling their susceptibility to death stimuli. In the present study, we investigated how human iPSCs react to DNA damage induced by several genotoxins and proapoptotic stimuli in comparison to fibroblasts. We found that iPSCs are hypersensitive to agents triggering the mitochondrial death pathway, which is mediated by the increased expression of several proapoptotic BCL-2 proteins. In contrast, iPSCs were largely resistant to death receptor-mediated apoptosis. Interestingly, despite the increased apoptosis sensitivity upon DNA damage, iPSCs displayed very low levels of DNA lesions compared to other cell types under diverse genotoxic conditions. Moreover, we found that iPSCs harbor high glutathione (GSH) levels and strongly express several GSH-dependent antioxidant enzymes. The combined depletion of GSH and glutathione peroxidase-2 (GPX2) levels was able to impair this iPSC-specific resistance to DNA damage. Thus, our results suggest that human iPSCs have a superior DNA maintenance response that is mediated by both an increased antioxidant defense and an elevated mitochondrial priming and apoptosis induction. These data might have profound implications for future iPSC-based therapies that are dependent on the quality of the differentiated cells and their ability to maintain an intact genome.

RESULTS

Human iPSCs Are Highly Susceptible to Mitochondrial Cell Death

To elucidate the relationship between DNA damage acquisition and apoptosis induction in human iPSCs, we first investigated the expression of pluripotency markers. Two iPSC lines that had been generated in our laboratory from adult skin fibroblasts (Lehle et al., 2014) were analyzed in more detail. In vitro analysis and morphological assessment showed that both iPSC lines were very similar to human ESCs and expressed alkaline phosphatase and pluripotency markers including NANOG, SOX2, TRA1-60, TRA1-81, and SSEA-4 (Figure S1). Moreover, visual observation revealed that no significant differentiation had occurred, even on the colony periphery.

As ROS generated during mitochondrial respiration are a major source of DNA damage (Schieber and Chandel, 2014), we first employed hydrogen peroxide to compare the cell death sensitivity of iPSCs and fibroblasts. After treatment with 500 μM H_2O_2, apoptotic and necrotic cell death was determined by fluorescence-activated cell sorting (FACS) measurement of annexin-V/propidium iodide (PI) staining. As shown Figure 1A, iPSCs were very sensitive to oxidative damage-induced cell death, whereas fibroblasts remained largely viable even after 24 hr of H_2O_2 treatment. A similar cell-type-specific sensitivity was observed after exposure to UVC light, a condition known to induce cell death mainly by oxidative DNA damage. Whereas iPSCs were already killed after exposure to a low UVC dose of 5 mJ/cm^2, their somatic precursor cells remained viable even after a high-dose UVC treatment of 100 mJ/cm^2 (Figure 1B). Furthermore, bleomycin, a genotoxic chemotherapeutic drug, efficiently induced cell death in iPSCs, but not in fibroblasts (Figure 1C).

The increased apoptosis sensitivity of human ESCs was reported to be selective to DNA-damaging stimuli (Dumitru et al., 2012). We therefore investigated cell death in response to non-genotoxic ER stress and applied tunicamycin and thapsigargin, which triggered cell death of iPSCs, but only weakly compromised the viability of fibroblasts (Figures 1D and 1E). In addition, brefeldin A, a Golgi complex disassembly agent, induced cell death in iPSCs, but not in fibroblasts (Figure 1F). Finally, we compared death receptor-mediated apoptosis in both cell types. Interestingly and in contrast to the previous stimuli, iPSCs remained largely resistant to FasL- or TRAIL-induced apoptosis even after prolonged incubation for 72 hr, whereas a considerable fraction of fibroblasts was already killed after a short exposure to both death ligands (Figures 1G and 1H). These results demonstrate that iPSCs display a high and selective apoptosis sensitivity to death stimuli activating the mitochondrial pathway, whereas they are largely resistant to death receptor-mediated apoptosis.

iPSCs Display Increased Mitochondrial Priming

To explore the mechanism underlying the low apoptosis threshold of iPSCs, we investigated the expression of several apoptosis mediators using qRT-PCR analysis (Figure 2A). Transcript levels of members of the inhibitor-of-apoptosis protein family, including *XIAP*, *IAP1*, and particularly *IAP2*, were considerably reduced in iPSCs compared to fibroblasts. In addition, iPSCs displayed lower mRNA expression of several antiapoptotic BCL-2 protein members, including *BCL2*, *BCLX*, *BCLW*, and *A1*. In contrast,

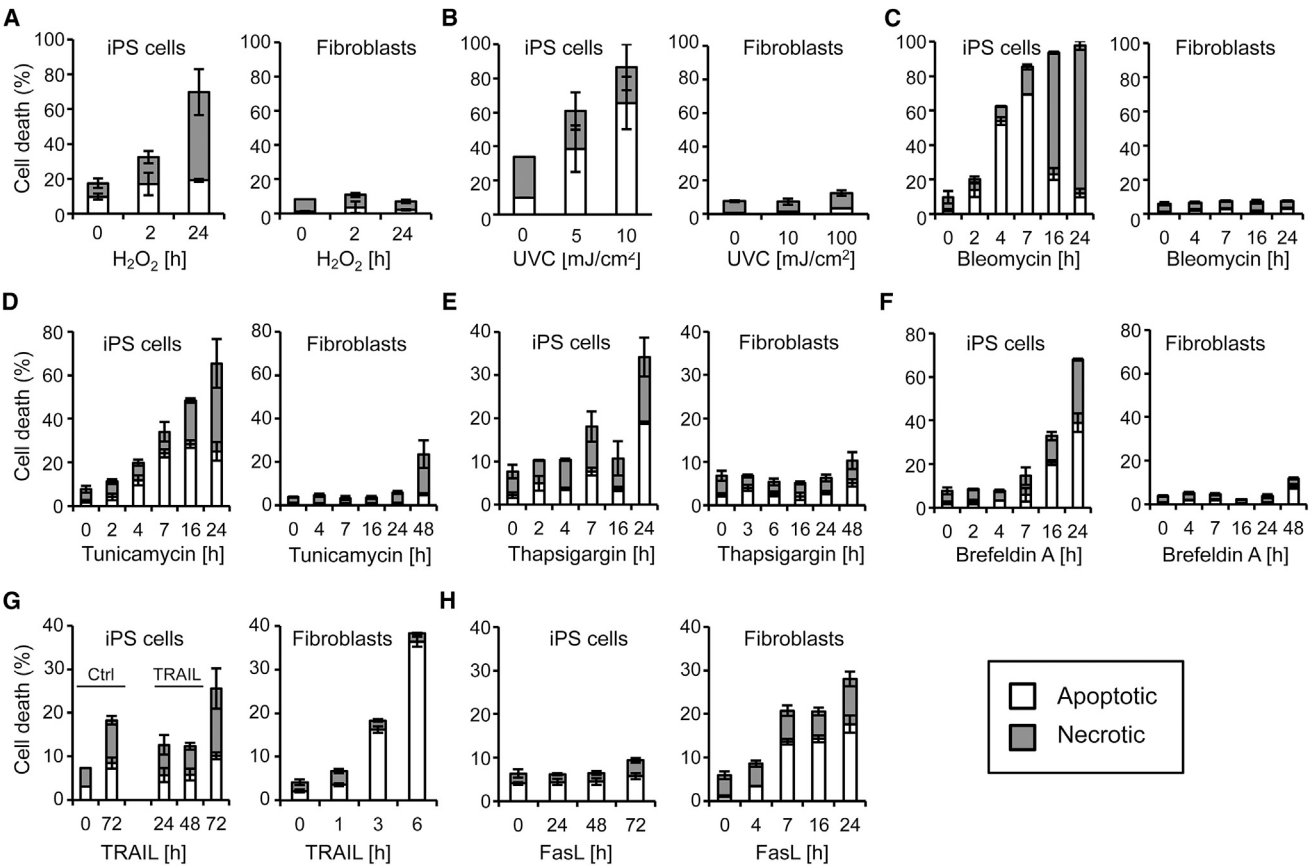

Figure 1. Human iPSCs Are Highly Susceptible to Stress Stimuli Triggering the Mitochondrial Death Pathway

(A–H) The human iPSC lines L1 and L2 and corresponding primary fibroblasts were treated for the indicated time with 500 μM H_2O_2 (A), 50 μM bleomycin (C), 6 μM tunicamycin (D), 1 μM thapsigargin (E), 1 μM brefeldin A (F), 50 ng/ml TRAIL (G), and 50 ng/ml FasL (H). In addition, cells were stimulated with the indicated dose of UVC 6 hr prior to cell death analysis (B). Apoptosis and necrosis rates were measured by annexin-V/PI staining. Results represent means ± SD from three independent experiments. ***p < 0.001.

even under basal conditions, *TP53* and important proapoptotic BCL-2 members, such as *BIM* and *NOXA*, were highly expressed in iPSCs compared to fibroblasts (Figure 2A). Furthermore, in line with previous cell death experiments, iPSCs expressed markedly reduced levels of the death ligand *TRAIL* as well as several death receptors (Figure 2B).

Since expression of BCL-2 proteins is often regulated by posttranslational events, we further analyzed protein expression using western blot analyses that revealed a high expression of p53 in iPSCs, but not in fibroblasts (Figure 2C). In addition, the p53-regulated proapoptotic proteins BAK and BIM were strongly expressed in iPSCs compared to fibroblasts. No significant differences between both cell types were found for BCL-X_L, BID, and BAX, whereas expression of MCL-1, which is regulated at the posttranslational level by Nanog (Noh et al., 2012), was elevated in iPSCs. Altogether, the mRNA and protein expression analyses indicated that iPSCs reveal an increased mitochondrial priming that is presumably mediated by a strong p53 response, resulting in a shift of the balance of antiapoptotic to proapoptotic BCL-2 proteins. In contrast, differentiated cells display low mitochondrial priming, resulting in resistance to DNA-damaging agents and other drugs activating the mitochondrial death pathway. Consistently, boosting the priming with the BH3 mimetic ABT-737 strongly sensitized fibroblasts to DNA damage-induced apoptosis (Figure 2D).

DNA Damage Rates in Genotoxically Stimulated iPSCs Are Lower Than in Fibroblasts and Increase upon Differentiation

Previous studies suggested that mechanisms of genome surveillance, including DNA repair, are superior in ESCs (Saretzki et al., 2008; Maynard et al., 2008). We therefore determined the accumulation of DNA damage in iPSCs and fibroblasts using long-run real-time PCR-based DNA damage quantification (LORD-Q) analysis, a highly sensitive technique for the detection of nuclear and mtDNA damage

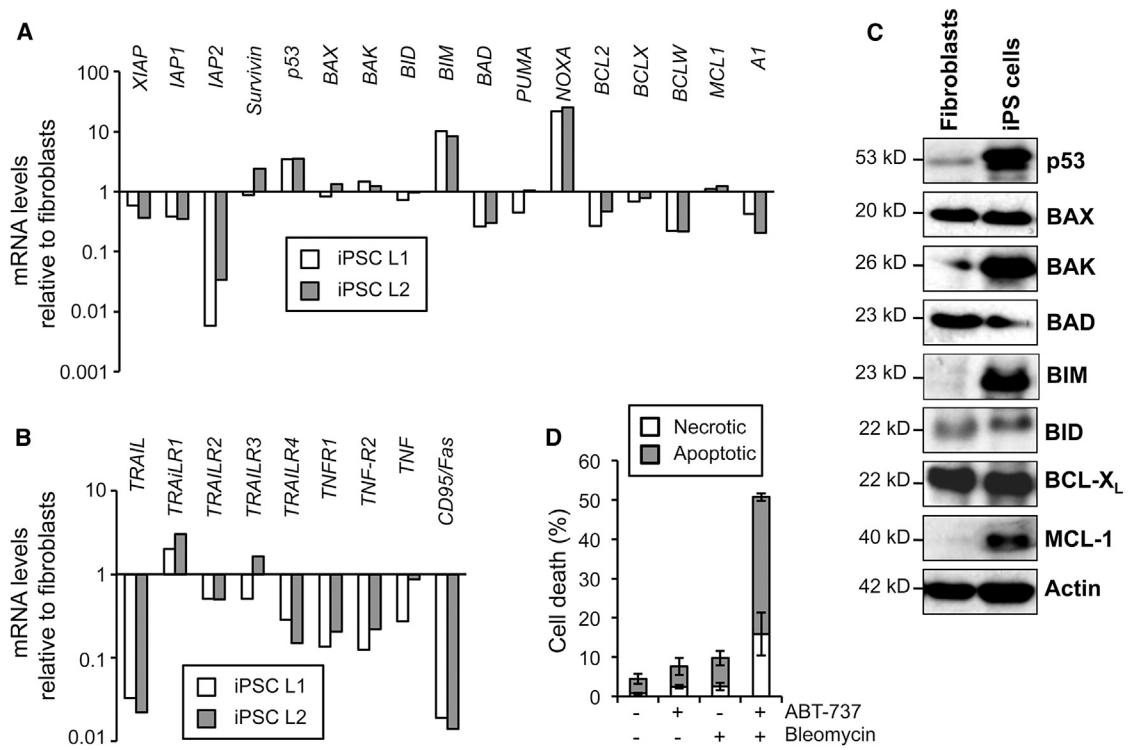

Figure 2. Human iPSCs Display Increased Mitochondrial Priming

(A and B) The iPSC lines L1 and L2 were analyzed for mRNA expression of the indicated regulators of the intrinsic (A) and extrinsic (B) apoptosis pathways relative to L2 fibroblast mRNA levels. *GAPDH* was used as reference. A representative experiment is shown.

(C) Western blot analysis shows p53 and the indicated members of the BCL-2 family in L2 iPSCs and fibroblasts.

(D) The BH3 mimetic BCL-2 inhibitor ABT-737 sensitizes fibroblasts to DNA damage-induced cell death. L2 fibroblasts were treated for 24 hr in the presence or absence of bleomycin (70 μM) and ABT-737 (25 μM). Apoptosis and necrosis were measured by annexin-V/PI staining. Results show the mean ± SD from three independent experiments.

(Lehle et al., 2014). To prevent apoptosis-mediated DNA fragmentation and cellular repair processes, we exposed the cells to UVC light, which induces DNA damage within a few seconds of treatment. Surprisingly and in contrast to the strong apoptotic response induced by UVC, accumulation of both nuclear and mtDNA lesions was significantly lower in iPSCs than in fibroblasts (Figure 3A). To verify these findings, we additionally measured oxidative DNA lesions, such as cyclobutane pyrimidine dimers and pyrimidine(6-4)pyrimidone photoproducts, using an ELISA, which confirmed the low accumulation of DNA damage in iPSCs (Figure 3B). Also, we analyzed mtDNA damage and the occurrence of 8-hydroxydeoxyguanosine (8-oxo-dG), a mutagenic DNA lesion, in response to H_2O_2 treatment, which also revealed a reduced acquisition of DNA lesions in iPSCs compared to fibroblasts (Figures 3C and 3D).

We next investigated whether this protection against DNA damage was maintained during iPSC differentiation. To induce differentiation, iPSCs were grown in fetal calf serum (FCS)-containing medium in the absence of FGF2. When fibroblasts and undifferentiated and differentiated iPSCs were exposed to different H_2O_2 concentrations, differentiated iPSCs clearly displayed enhanced DNA damage rates compared to their undifferentiated counterparts (Figure 3E). Thus, protection of pluripotent cells against DNA damage is rapidly lost upon differentiation.

Human iPSCs Exhibit Significantly Lower DNA Lesion Rates Than Most Tumor Cell Lines

Since malignant cells exhibit several features of stem cells, we wanted to investigate whether the protection against DNA damage also could be observed in tumor cells. In addition to iPSCs and fibroblasts, we therefore UVC-irradiated 15 different tumor lines that were mostly derived from the NCI60 panel. We found that iPSCs exhibited a significantly lower DNA damage rate than fibroblasts in all three investigated genomic loci, namely mtDNA (Figure 4A), the *GAPDH* locus (Figure 4B), and the *TP53* locus (Figure 4C). In most tumor cell lines, the levels of nuclear and mtDNA damage correlated with each other. Moreover, the damage rate of mtDNA and the two examined nuclear loci was significantly lower in iPSCs than in most tumor cell lines.

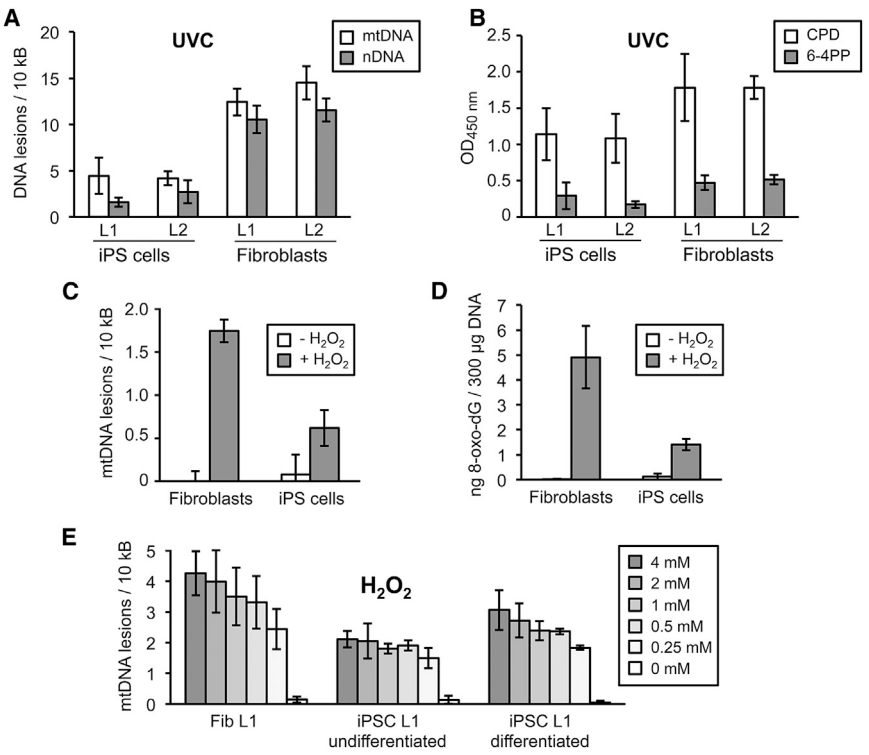

Figure 3. Human iPSCs Are Protected against Mitochondrial and Nuclear DNA Damage

(A) The iPSC lines L1 and L2 and corresponding fibroblasts were irradiated with 20 mJ/cm^2 UVC light. Immediately after irradiation, damage of mitochondrial (mtDNA) and nuclear DNA (nDNA; *GAPDH* locus) was determined by LORD-Q analysis. Results show mean values ± SD from three independent experiments. $p = 0.005$ (L1 mtDNA), $p < 0.001$ (L2 mtDNA, L1 nDNA, and L2 nDNA).

(B) Following UVC irradiation (20 mJ/cm^2) of iPSCs and fibroblasts, DNA samples were analyzed for cyclobutane pyrimidine dimers (CPD) and pyrimidine(6-4)pyrimidone photoproducts (6-4PP) by ELISA. Results show mean values ± SD from three independent experiments. $p < 0.05$.

(C) The iPSCs and fibroblasts were exposed to 5 mM H_2O_2 for 5 min before mtDNA damage was measured by LORD-Q analysis. Results show mean values ± SD, which were obtained from L1 and L2 iPSCs and the corresponding fibroblasts in three independent experiments. $p < 0.002$.

(D) The iPSCs and fibroblasts were exposed to 5 mM H_2O_2 for 5 min before DNA samples were analyzed for 8-oxo-dG lesions. Results show mean values ± SD, which were obtained from L1 and L2 iPSCs and the corresponding fibroblasts in three independent experiments. $p < 0.001$.

(E) L1 fibroblasts, undifferentiated iPSCs, and iPSCs that had been differentiated by 30 days of incubation in the presence of FCS and absence of FGF2 were treated for 5 min with the indicated concentrations of H_2O_2. mtDNA damage rates were measured by LORD-Q analysis and are given as mean ± SD from three independent experiments. Comparison of whole datasets of undifferentiated iPSCs with data of fibroblasts and differentiated iPSCs resulted in p values of $p < 0.001$ and $p = 0.002$, respectively.

Thus, during genotoxic exposure, iPSCs acquire less DNA lesions than parental fibroblasts and cells derived from various tumor entities.

Human iPSCs Display High GSH Levels and Decreased Oxidative Stress

Reduced DNA damage could be mediated by increased expression of DNA repair genes, as previously shown in ESCs (Saretzki et al., 2008; Maynard et al., 2008). However, since iPSCs exhibit protection against both nuclear and mtDNA damage, another explanation could be that there is less oxidative damage occurring, possibly due to higher levels of antioxidants. Measurement of the levels of GSH, the most important cellular antioxidant, indeed revealed 3- to 4-fold increased levels of GSH in iPSCs compared to fibroblasts (Figure 5A). To investigate the functional role of increased GSH levels, we depleted cellular GSH using dimethyl fumarate (DMF), which is metabolized in a GSH-dependent manner, and buthionine sulfoximine (BSO), an irreversible γ-glutamylcysteine synthetase inhibitor. Combined treatment of iPSCs and fibroblasts with both agents for 1 hr was sufficient to reduce GSH contents in both cell types by at least 80%, without inducing cell death (Figure 5B). When cells were subsequently treated with H_2O_2, GSH-depleted fibroblasts exhibited a significant and strong increase in DNA damage that was partially reversed by a cell-permeable glutathione O-ethylester (GSH-OEt) (Figure 5C). Surprisingly, however, only minor effects of GSH depletion and substitution on DNA lesion rates were observed in iPSCs (Figure 5C).

To investigate whether the cells had experienced comparable intracellular stress levels, we measured ROS levels using dihydrorhodamine 123 staining and FACS analysis. As shown in Figure 5D, both cell types displayed considerable ROS level increases after H_2O_2 exposure, which was significantly boosted by GSH depletion and rescued by GSH O-ethylester, demonstrating that the experimental setup was not responsible for the low effect of GSH depletion on the DNA vulnerability of iPSCs. Notably, the increase of ROS levels in fibroblasts was 5- to 10-fold higher than in iPSCs, suggesting that oxidative stress is efficiently prevented in iPSCs.

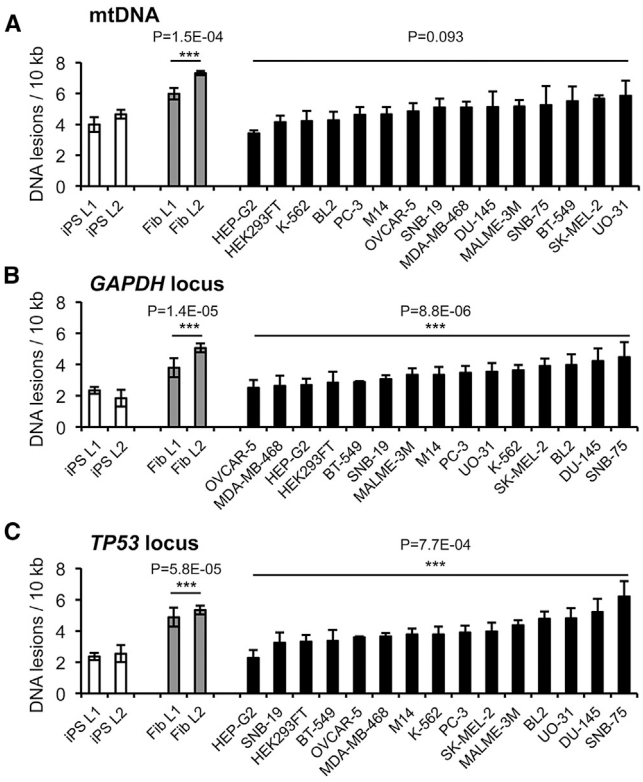

Figure 4. Comparison of DNA Damage Rates in iPSCs, Fibroblasts, and Tumor Cell Lines

(A–C) The human iPSC lines L1 and L2, corresponding fibroblasts, and several human cell lines of different tumor entities were irradiated with 10 mJ/cm^2 UVC light. Immediately after irradiation, cells were harvested and mtDNA damage (A) and nDNA damage in the *GAPDH* (B) and *TP53* locus (C) were quantified using LORD-Q analysis. P values indicate statistical significance between iPSCs and fibroblast and tumor cell lines, respectively.

High Levels of GPX2 and GSH Protect iPSCs from DNA Damage

The previous results indicated that iPSCs exhibit high GSH levels, but might possess additional safeguard mechanisms. We therefore analyzed mRNA expression of several antioxidant enzymes in fibroblasts and iPSCs (Figure 6). Our qRT-PCR analyses revealed that several glutathione S-transferases (GSTs), which act as antioxidant and detoxifying enzymes, were upregulated in iPSCs compared to their somatic precursor cells. Most striking was *GSTA2* that was expressed at more than 80,000-fold higher levels in iPSCs relative to primary fibroblasts. In addition, iPSCs revealed a more than 10,000-fold higher expression of *GPX2*. Furthermore, several peroxiredoxins, which act as scavengers of H_2O_2 and organic hydroperoxides, as well as glutathione reductase were considerably upregulated in iPSCs, supporting the potent antioxidant status of iPSCs (Figure 6).

In iPSCs the transcript levels of *GSTA2* and *GPX2* were elevated not only compared to fibroblasts but also compared to most tumor cell lines (Figure 7A). The sole exception was observed in HepG2 hepatocellular carcinoma cells that, as typical for liver cells, expressed not only increased levels of both enzymes (Figure 7A), but were also relatively resistant to DNA damage (Figure 4). To investigate a functional contribution of GSTA2 or GPX2 to DNA damage protection, we reduced mRNA levels of both enzymes in iPSCs by small interfering RNA (siRNA) treatment. However, neither *GSTA2* nor *GPX2* knockdown alone led to significant increases of detectable DNA damage following H_2O_2 exposure (Figure 7B). We next combined GSH depletion with the knockdown of *GPX2* or *GSTA2* in iPSCs. In GSH-depleted cells, knockdown of *GPX2*, but not of *GSTA2*, significantly rendered the cells more vulnerable to DNA damage following H_2O_2 exposure. Vice versa, the lentiviral overexpression of GPX2 in fibroblasts was sufficient to confer increased resistance to DNA damage (Figure 7C). These results thus indicate that high levels of GSH and GPX2 mediate DNA damage protection of iPSCs. In view of the increased expression of several other antioxidant mediators as well as the reported abundance of DNA repair proteins, it is likely that, in addition, further DNA damage protection mechanisms ensure genomic integrity of iPSCs.

DISCUSSION

Pluripotent stem cells must tightly control the balance between cell survival and death to prevent unfavorable mutations and to ensure genomic integrity. First, maintenance of genomic stability must be particularly stringent, because any genetic alterations in pluripotent stem cells can impair the functionality of their progeny and compromise tissue renewal. Pluripotent stem cells bear an enhanced tumorigenic potential and share several characteristics with cancer cells, such as replicative immortality (Ben-David and Benvenisty, 2011). These properties require a quick and strong apoptotic response in DNA-damaged cells to prevent an accumulation of mutations that could facilitate deregulated proliferation or predispose cells to acquire further mutations associated with cancer development.

It has been shown that ESCs are hypersensitive to DNA damage and readily undergo apoptosis (Qin et al., 2007; Madden et al., 2011; Liu et al., 2013), although much less is known about iPSCs. DNA damage sensitivity in human ESCs was shown to correlate with a property, termed mitochondrial priming, that is determined by the balance between pro- and antiapoptotic BCL-2 proteins (Liu et al., 2013). In the present study, we found that, compared to differentiated fibroblasts, iPSCs exhibit a low apoptosis

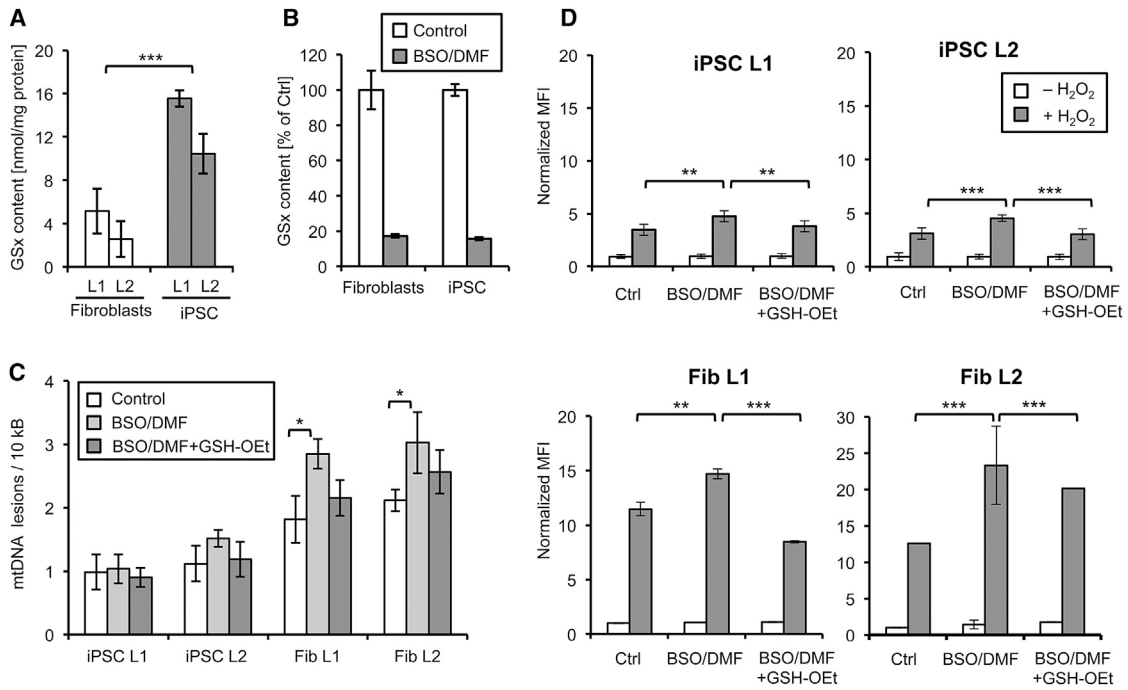

Figure 5. Human iPSCs Have High GSH Levels and Decreased Oxidative Stress

(A) Analysis of total GSH (GSx) levels in iPSCs and fibroblasts. Values show means ± SD from three independent experiments.

(B) Combined treatment of iPSCs and fibroblasts with 100 μM DMF and 100 μM BSO for 1 hr strongly reduces GSH levels. Values show means ± SD from three independent experiments.

(C) Effect of GSH depletion on H_2O_2-induced mtDNA damage. GSH-depleted iPSCs and fibroblasts were treated for 5 min with 2 mM H_2O_2 before mtDNA damage was determined by LORD-Q analysis. GSH depletion significantly increased H_2O_2-induced mtDNA lesions in fibroblasts, but not in iPSCs. Sensitization was partially reversed by supplementation with 2 mM GSH-OEt. Results show means ± SD from three independent experiments.

(D) Oxidative stress levels in iPSCs and fibroblasts. GSH-depleted, GSH-OEt-supplemented, BSO/DMF-treated, and control cells were stained with dihydrorhodamine 123 prior to H_2O_2 exposure (2 mM, 5 min) and analyzed by flow cytometry. ROS levels are shown as values of normalized mean fluorescence intensity (MFI) from three independent experiments. *$p < 0.05$, **$p < 0.01$, ***$p < 0.001$.

threshold. Interestingly, the high apoptosis sensitivity was restricted to stimuli activating the mitochondrial pathway, whereas iPSCs were strongly resistant to the extrinsic apoptosis pathway, presumably by the downregulation of several death receptors. Unlike human ESCs (Dumitru et al., 2012), however, the increased sensitivity of iPSCs was not confined to DNA-damaging stimuli, but also observed after treatment with ER stress- or Golgi disassembly-inducing agents that also trigger the mitochondrial pathway.

Human ESCs have been reported to maintain BAX in an active conformation at the Golgi apparatus under basal conditions (Dumitru et al., 2012), but this mechanism is unlikely the sole reason of their increased apoptosis sensitivity. In support of this notion is the finding that the H1 ESC line displays the typical apoptosis hypersensitivity, but lacks expression of active BAX at the Golgi (Dumitru et al., 2012). Moreover, we found that, also in human iPSCs, BAX was evenly distributed in the cytosol, but was not localized at the Golgi (Figure S2). Nevertheless, our results showed that, even under basal conditions, iPSCs reveal a strong accumulation of p53, a tumor suppressor, which also acts as a barrier to somatic cell reprogramming (Tapia and Schöler, 2010). p53 activates the transcription of multiple genes involved in apoptosis, in particular pro-apoptotic BCL-2 proteins. Indeed, compared to fibroblasts, expression of several p53 target genes including *BAK*, *BIM*, and *NOXA* was strongly upregulated, indicating that iPSCs exhibit high mitochondrial priming compared to differentiated cells. Fibroblasts, however, could be sensitized to DNA damage-induced apoptosis using ABT-737, an inhibitor of antiapoptotic BCL-2 proteins.

In addition to apoptosis, we investigated the occurrence of DNA lesions in response to genotoxic insults. Using LORD-Q analyses, a novel sensitive technique to quantify DNA lesions (Lehle et al., 2014), we found that, despite their elevated apoptosis sensitivity, iPSCs accumulated significantly less DNA lesions than differentiated

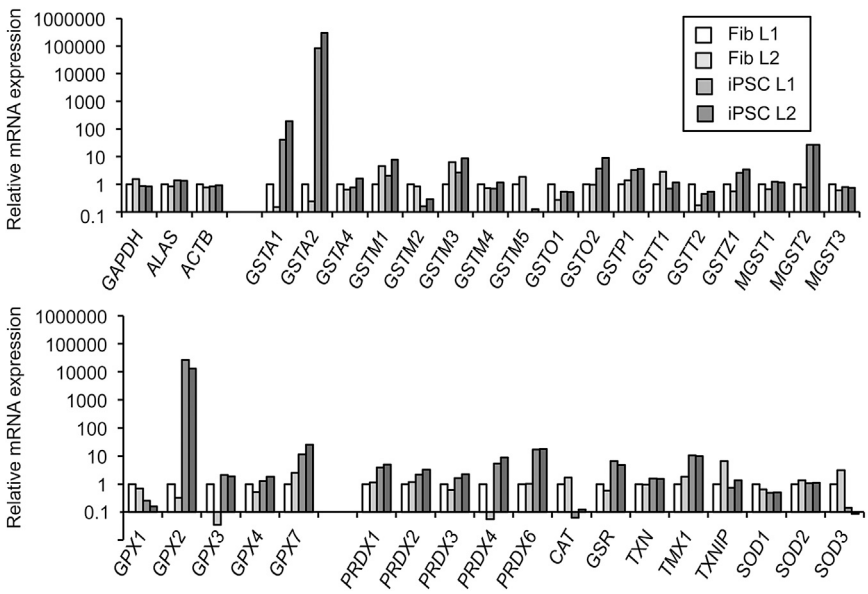

Figure 6. Increased mRNA Expression of Antioxidant and Detoxifying Enzymes in iPSCs

The iPSCs and fibroblasts were screened for the differential expression of factors involved in cellular ROS detoxification by qRT-PCR. mRNA expression in L1 fibroblasts was set as 1. A representative dataset is shown. *GAPDH*, GAPDH glyceraldehyde-3-phosphate dehydrogenase; *ALAS*, amino-levulinate synthase; *ACTB*, beta-actin; *GST*, glutathione S-transferase; *MGST*, microsomal GST; *GPX*, glutathione peroxidase; PRDX, peroxiredoxin; *CAT*, catalase; *GSR*, GSH reductase; *TXN*, thioredoxin; *TMX1*, thioredoxin-related transmembrane protein 1; *TXNIP*, thioredoxin-interacting protein; *SOD*, superoxide dismutase.

fibroblasts. Also, in response to treatment with H_2O_2 and UVC, oxidative nucleotide modifications such as cyclobutane pyrimidine dimers, (6-4) photoproducts, and 8-hydroxydeoxyguanosine (8-oxo-dG) were detected less frequently. Thus, our data are consistent with the hypothesis that pluripotent stem cells have superior DNA maintenance responses. Interestingly, we observed that this DNA damage protection was rapidly lost during differentiation of iPSCs.

There are presumably several mechanisms that contribute to an efficient maintenance of DNA integrity in pluripotent stem cells, including the prevention of DNA damage and the removal of DNA lesions. Compared to differentiated cells, ESCs display a moderate increase (approximately 2- to 3-fold) in the expression of certain DNA repair enzymes of the homologous recombination and non-homologous end-joining pathways, which repair DNA double-strand breaks (Saretzki et al., 2008). It is interesting to note that a previous study in human ESCs (Maynard et al., 2008) found decreased levels of oxidative DNA lesions, such as 8-oxo-dG, which we assessed as an additional marker of DNA damage in iPSCs. Although the decreased 8-oxo-dG levels are suggestive of a more efficient repair of this lesion, the authors did not find elevated activities of 8-oxoguanine glycosylase, the primary base excision repair enzyme required for removing this mutagenic DNA lesion. These results indicate that base excision repair is presumably not elevated in ESCs, but rather the occurrence of oxidative DNA lesions is prevented.

Our study shows that iPSCs are highly proficient in antioxidant defense, which is presumably responsible for the low frequency of oxidative DNA lesions in both the mitochondrial and nuclear genome. Notably, previous non-quantitative proteomic studies revealed an abundant expression of antioxidant enzymes, in particular several peroxiredoxins in human ESCs (Baharvand et al., 2006). Furthermore, ESC cultures generate fewer ROS than most somatic cell types, because of their lower reliance on oxidative phosphorylation and limited mitochondrial biogenesis (Prigione et al., 2010; Armstrong et al., 2010). Structural analyses of mitochondria in human ESCs demonstrated an immature network characterized by few organelles with poorly developed cristae, which however increase during differentiation (St John et al., 2006; Facucho-Oliveira et al., 2007). Thus, stem cells maintain low ROS levels not only by high antioxidant activity, but also by reduced oxygen consumption and low mitochondrial biogenesis. Our PCR-based LORD-Q method enabled us to specifically assess not only nuclear but also mtDNA lesions. Several lines of evidence suggest that, in particular, the occurrence of mtDNA lesions must be prevented for the maintenance of pluripotency. For instance, studies in a mouse model with high levels of mtDNA mutations due to a proof-reading defect of DNA polymerase γ (mtDNA mutator mice) established causal relationships among the accumulation of mtDNA mutations, stem cell exhaustion, and premature aging (reviewed in Baines et al., 2014).

In our study, we found that the level of GSH, the most important cellular antioxidant, was elevated up to 4-fold in iPSCs compared to somatic fibroblasts. In addition, the mRNA levels of several peroxiredoxins, GSTs, and glutathione reductase were considerably increased. All these enzymes might be involved in antioxidant defense and detoxification, a finding reminiscent of the expression of aldehyde dehydrogenase-1, which is often used as marker of cancer stem cells (Ginestier et al., 2007).

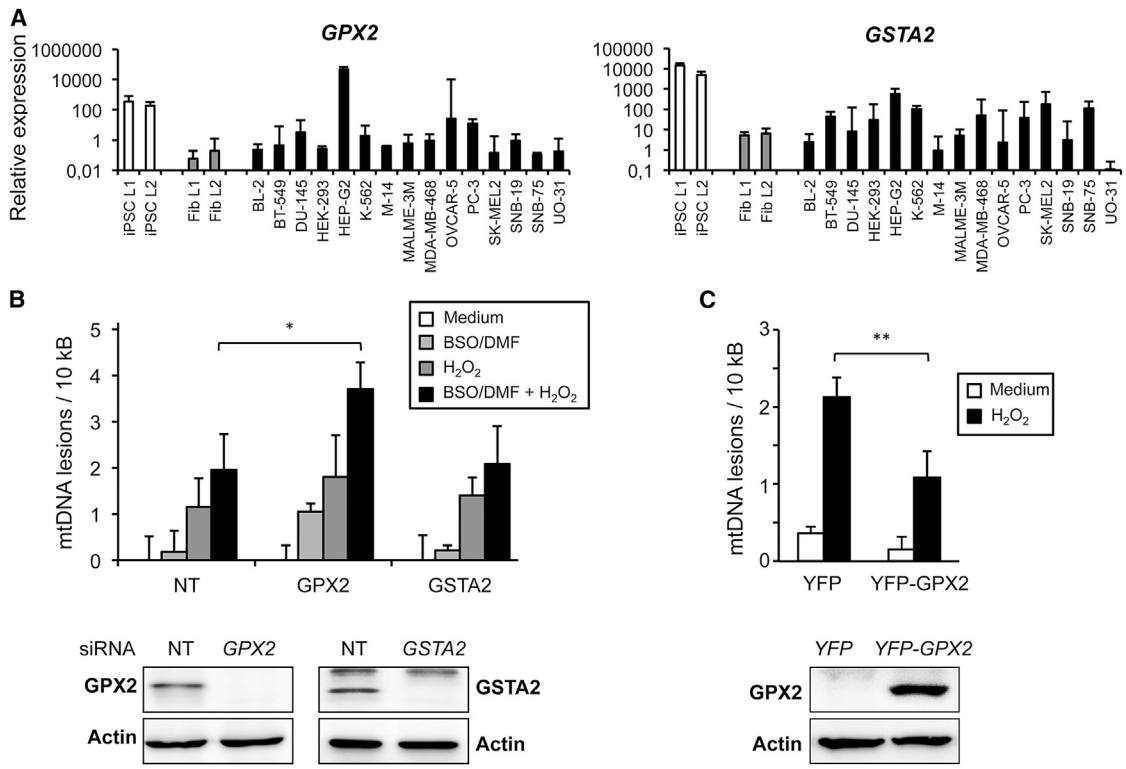

Figure 7. GPX2 and GSH Contribute to DNA Damage Protection in iPSCs

(A) Transcript levels of *GPX2* and *GSTA2* in iPSCs, fibroblasts, and cell lines of different tumor entities. The mRNA levels of the two GSH-dependent enzymes were analyzed by qRT-PCR relative to *GAPDH*. A representative dataset is shown.

(B) Combined GSH depletion and *GPX2* knockdown impair DNA damage protection of iPSCs. L2 iPSCs were incubated with 25 nM *GPX2*-specific, *GSTA2*-specific, or non-targeting (NT) siRNA. After 72 hr, GSx was depleted by the addition of BSO/DMF for 1 hr, followed by exposure to 2 mM H_2O_2 for 5 min. (Top) Measurement of mtDNA damage using the LORD-Q assay is shown. Results represent means ± SD of three independent experiments. *$p < 0.05$. (Bottom) Confirmation of the GPX2 and GSTA2 knockdown by western blotting is shown.

(C) Overexpression of GPX2 is sufficient to confer increased resistance to DNA damage in fibroblasts. L2 fibroblasts were transduced with lentiviral vectors for YFP-coupled GPX2 or the YFP control. Then, 48 hr post-infection, cells were treated with 2 mM H_2O_2 for 5 min. (Top) Measurement of mtDNA damage by LORD-Q analysis is shown. Results represent means ± SD from three independent experiments. $p = 0.002$. (Bottom) Confirmation of GPX2 overexpression by western blotting using an anti-GPX2 antibody is shown.

Most notable was our finding that expression of two GSH-dependent enzymes, *GSTA2* and *GPX2*, was elevated more than 80,000- and 10,000-fold, respectively, compared to fibroblasts. We therefore investigated their possible contribution to the maintenance of genomic integrity. Our data show that overexpression of GPX2 in fibroblasts can significantly increase resistance to oxidative stress-induced DNA damage. Moreover, using RNAi, we found that knockdown of *GPX2*, but not *GSTA2*, could overcome DNA damage protection in iPSCs. However, combined depletion of GSH was required for sensitization to DNA damage, indicating that, in addition to GPX2, further antioxidant mechanisms might be involved in the protection against DNA damage in iPSCs. This assumption is supported by our finding that the expression of several antioxidant enzymes was strongly increased in iPSCs.

Although GPX2 is known as a gastrointestinal GSH peroxidase, it also is expressed in other tissues (Brigelius-Flohé and Kipp, 2012). Interestingly, its expression level is increased in intestinal crypt stem cells and malignant epithelial cells, suggesting a role in proliferation and self-renewal. It also was found that GPX2 overexpression alleviates the apoptotic response of breast cancer cells to oxidative stress (Yan and Chen, 2006). The *GPX2* promoter is activated by the Wnt pathway that is highly active in iPSCs and ESCs (Kipp et al., 2012). Like many antioxidant enzymes, GPX2 expression is further controlled by transcription factor NRF2 (Banning et al., 2005), which very recently has been implicated also in the self-renewal capacity of ESCs (Jang et al., 2014). It is thus conceivable that the high antioxidant defense of iPSCs is not only involved in genomic stability, but also required for self-renewal,

replicative immortality, and the delay of differentiation of iPSCs.

In summary, our study brings together two seemingly separate processes that accompany the function of iPSCs. Human iPSCs are able to defend their genomic integrity by maintaining low levels of ROS through a combination of enhanced removal and limited production of these molecules. In addition to the endowance with superior DNA repair systems, iPSCs display high mitochondrial priming and apoptosis sensitivity, once DNA damage has occurred. These processes might not only ensure genomic stability and prevent transmission of mutations to the progeny, but also might be important for a possible therapeutic application of iPSCs.

EXPERIMENTAL PROCEDURES

Cell Culture

Human iPSCs were generated as described (Takahashi et al., 2007; Lehle et al., 2014) by transduction of dermal fibroblasts with the Yamanaka retroviral cocktail, and grown on mitotically inactivated mouse embryonic fibroblast (MEF) feeder cells in hES medium containing Knockout DMEM, 20% serum replacement (all from Life Technologies), 2 mM glutamine, non-essential amino acids, 25 μM 2-mercaptoethanol, and 5 ng/ml FGF2 (PeproTech). Human fibroblasts were cultured in RPMI-1640 supplemented with 10% FCS, 2 mM glutamine, and 2 mM sodium pyruvate. All other cell lines were obtained from ATCC and grown in the recommended media. Culture media were supplemented with penicillin/streptomycin.

Microscopy

For characterization of the iPSCs, cells were stained for the expression of pluripotency markers, including NANOG, SOX2, TRA1-60, TRA1-81, and SSEA-4. To this end, cells were fixed with ice-cold acetone/methanol (1:1) for 5 min, washed with PBS, and incubated for 1 hr in blocking buffer (4% BSA, 0.05% saponin in PBS) at room temperature. The primary antibodies (listed in Table S1) were incubated at 4°C overnight. After washing the cells thrice in blocking buffer, the appropriate Alexafluor-coupled secondary antibody was applied for 1 hr. Cells were washed again in PBS and incubated afterward in PBS containing 100 ng/ml DAPI for 5 min. Coverslips were mounted in fluorescence mounting medium and analyzed using a DMI6000 fluorescence microscope (Leica). Alkaline phosphatase activity was determined by the Alkaline Phosphatase Detection kit (Millipore) after fixation of cells with 4% formaldehyde. For detection of active BAX at the Golgi, cells were fixed in formaldehyde, permeabilized in blocking buffer, and stained with conformation-specific anti-BAX-NT and the Golgi marker anti-GM130.

Cell Death Analysis

Cells were stimulated with the indicated genotoxic and proapoptotic agents, including bleomycin (Medac), hydrogen peroxide, thapsigargin, tunicamycin, brefeldin A (all from Sigma), as well as recombinant TRAIL and FasL (both from Enzo Life Sciences). After cell harvest using trypsin for differentiated cells and accutase (Millipore) for iPSCs, supernatants containing dead cells and the detached cells were combined. Subsequently, cells were stained with FITC-annexin-V and PI following the instructions of the manufacturer (BD Biosciences) and analyzed by flow cytometry. Cells with positive annexin-V but negative PI staining were considered apoptotic, whereas double-positive cells were considered necrotic.

Induction and Detection of DNA Damage

For induction of DNA damage, adherent somatic cells were singularized using trypsin/EDTA. The iPSCs were detached by accutase in the presence of the ROCK inhibitor Y-27632 (10 μM, Wako Pure Chemicals Industries) for 10 min at 37°C. Then, 1×10^6 cells were resuspended in PBS supplemented with 5% FCS (PBS/F). UVC irradiation was carried out in 100-mm culture dishes and 10 ml PBS/F using a Stratalinker 2400 (Stratagene). Bleomycin exposure was carried out in 300 μl PBS/F for 20 min. H_2O_2 treatment was performed in 1 ml PBS for 5 min at 37°C. Immediately after stimulation, cells were collected by centrifugation and snap-frozen in liquid nitrogen.

Detection and quantification of DNA damage was performed by ELISA or LORD-Q analyses as described previously (Lehle et al., 2014). Briefly, whole-cell DNA was isolated from genotoxin-exposed and control samples using the DNeasy Blood & Tissue kit (QIAGEN) and diluted to 10 ng/μl by the addition of suitable volumes of elution buffer. Subsequently, 5 μl diluted sample DNA was added to 15 μl master mix consisting of 10 μl 2× KAPA2G Fast Hot Start Polymerase, 1 μl sense and 1 μl antisense primer (containing each 10 pmol of the respective oligonucleotide), 0.05 μl 20× LightCycler 480 ResoLight Dye (Roche), and 2.95 μl high-performance liquid chromatography (HPLC)-grade water. For each analyzed genomic locus, a long DNA damage sensor fragment and a short reference DNA fragment were amplified in two separate real-time PCR runs (5 min at 95°C pre-heating phase followed by 50 PCR cycles: 10 s 95°C, 10 s 60°C, 2:15 min [long fragments] or 1 s [short fragments] at 72°C). For nuclear DNA damage determination, the *GAPDH* and *TP53* loci were analyzed (see Table S2 for primer sequences). Calculation of detected lesions per 10 kb was performed as described previously (Lehle et al., 2014). DNA lesions such as cyclobutane pyrimidine dimers, (6-4) photoproducts, and 8-hydroxydeoxyguanosine were measured using ELISA kits from Cell Biolabs.

Western Blot Analyses

Cells were washed in ice-cold PBS and resuspended in 100–200 μl RIPA buffer supplemented with 1× Mini Complete Protease Inhibitor cocktail (Roche). Protein concentrations were determined by the BCA assay and 10–50 μg protein per lane was loaded onto SDS-PAGE gels. After electrophoresis, proteins were transferred onto polyvinylidenedifluoride membranes (Amersham Biosciences). Membranes were blocked in PBS containing 4% BSA and 0.05% Tween-20 for 1 hr, followed by an overnight incubation with the primary antibodies (listed in Table S1) in blocking buffer at 4°C. After washing the membrane thrice in Tris-buffered saline (TBS)/0.05% Tween, peroxidase-coupled secondary antibodies

were applied for 1 hr. Proteins were visualized using enhanced chemiluminescence (ECL) reagents (Amersham Biosciences).

qRT-PCR

For relative expression analysis, RNA was isolated from cell pellets using the RNeasy Mini Kit (QIAGEN). After reverse transcription (Transcriptor First Strand cDNA Synthesis kit, Roche), cDNA levels were analyzed in a real-time PCR approach. Experiments were carried out in 96- or 384-well plates on a LightCycler 480 II system (Roche). Per reaction (96-well plates: 20 µl; 384-well plates: 10 µl reaction), 10 µl 2× SYBR Green master mix (Fermentas), each 10 pmol sense and antisense primer (see Table S3 for primer sequences), 10 ng of sample cDNA, and HPLC-grade water (ad 20 µl) were used. The real-time PCR program comprised a 5-min heating phase (95°C) followed by 35 to 50 cycles (10 s at 95°C, 10 s at 60°C, 10 s at 72°C). Relative transcript levels were calculated using the $2^{-\Delta\Delta C_T}$ method (Livak and Schmittgen, 2001). Glyceraldehyde dehydrogenase (*GAPDH*), beta-actin (*ACTB*), and delta-aminolevulinate synthetase 1 (*ALAS1*) were used as reference genes. Each sample was analyzed in triplicate and the resulting C_p values were averaged.

Manipulation and Analysis of Cellular GSH Content

Total cellular GSH (GSx; c[GSx] = c[GSH] + 2 × c[GSSG]) content was determined as described previously (Tietze, 1969). Briefly, 10^5 to 10^6 cells were lysed in ice-cold 1% 5-sulfosiacylic acid. After 30-min incubation on ice, lysates were centrifuged (10 min, 20,000 × *g*) and the supernatants were used for GSx determination, while the pellets were analyzed for protein content by the BCA assay. Then, 10 µl supernatants were transferred to a 96-well plate and mixed with 100 µl reaction solution containing 0.64 µl glutathione reductase (Sigma) solution, 400 µM NADPH, 300 µM of the colorimetric dye 5,5′-dithiobis-(2-nitrobenzoic acid), and 2 mM EDTA in 100 mM sodium phosphate buffer (pH 7.5). Subsequently, the absorption at 412 nm was followed for 10 to 15 min and the slopes of the resulting curves were determined. GSx concentrations were calculated using standard curves, normalized for protein content and expressed as nmol GSx/mg protein. Depletion of cellular GSx pools was achieved by co-incubation of the cells with 100 µM DMF (Sigma) and 100 µM BSO (Sigma) for up to 4 hr (Boivin et al., 2011). GSH repletion was performed by co-incubation of cells with BSO/DMF and 2 mM GSH-OEt (Sigma) (Ghoreschi et al., 2011).

Determination of ROS Levels

To measure intracellular ROS, 3 × 10^5 cells were stained with 1 µM dihydrorhodamine 123 (Sigma) in PBS for 10 min at 37°C. Subsequently, cells were pelletized and resuspended in PBS. Stimulation with 2 mM H_2O_2 was performed for 5 min at 37°C. After centrifugation, cells were resuspended in PBS/F and analyzed by flow cytometry.

Gene Knockdown via siRNA

The iPSCs (5 × 10^5–10^6) were harvested with accutase supplemented with 10 µM ROCK inhibitor Y-27632 as described above. Subsequently, the protocol of Ma et al. (2010) was followed. Briefly, cells were resuspended in 100 µl OPTIMEM medium (Invitrogen) supplemented with 400 nM SMARTpool siRNA (Dharmacon) and 5 µl lipofectamine 2000 (Invitrogen). The cell suspension was incubated for 5 min at 37°C, then diluted with 1.5 ml culture medium and transferred into six-well plates coated with feeder MEFs. Cells were harvested 72 hr post-transfection and stimulated with the indicated genotoxic agents.

Overexpression of GPX2 in Human Dermal Fibroblasts

A third-generation lentiviral expression system was used to overexpress YFP-tagged GPX2 and YFP, respectively, in human dermal fibroblasts. The lentiviral vectors pLV.YFP and pLV.YFP-GPX2 were kindly provided by O. Kranenburg (University Medical Center, Utrecht, the Netherlands) and co-transfected with pMDLg, pRSV-Rev, and pMD2.G vector constructs (Addgene) into HEK293 cells using jetPEI (Polyplus). Virus was harvested 2 days post-transfection. The fibroblasts were incubated with virus-containing medium for 24 hr, and infected cells were selected with 5 µg/ml puromycin 48 hr following infection.

SUPPLEMENTAL INFORMATION

Supplemental Information includes two figures and three tables and can be found with this article online at http://dx.doi.org/10.1016/j.stemcr.2015.04.004.

AUTHOR CONTRIBUTIONS

B.D, S.L., O.R., and K.S.-O. conceived and designed the study, performed data analysis, and wrote the paper. B.D., S.L., D.G.H., A.K., P.G., V.S., K.H., M.F., and F.E. performed experiments and assembled the data.

ACKNOWLEDGMENTS

We thank Karen J. Nieken and Marie Baur for technical assistance, Anna P. Kipp for the GPX2 antibody, John Hayes for the GSTA2 antibody, and Jamilla Laoukili and Ono Kranenburg for GSTA2 expression constructs. This work was supported by the Deutsche Forschungsgemeinschaft (SFB 773, SFB 685, and GRK 1302). S.L. was funded by the Innovation Grant of the Excellence Initiative of the University of Tübingen and Alfred Teufel Foundation.

Received: October 14, 2014
Revised: April 3, 2015
Accepted: April 3, 2015
Published: April 30, 2015

REFERENCES

Armstrong, L., Tilgner, K., Saretzki, G., Atkinson, S.P., Stojkovic, M., Moreno, R., Przyborski, S., and Lako, M. (2010). Human induced pluripotent stem cell lines show stress defense mechanisms and mitochondrial regulation similar to those of human embryonic stem cells. Stem Cells *28*, 661–673.

Baharvand, H., Hajheidari, M., Ashtiani, S.K., and Salekdeh, G.H. (2006). Proteomic signature of human embryonic stem cells. Proteomics *6*, 3544–3549.

Baines, H.L., Turnbull, D.M., and Greaves, L.C. (2014). Human stem cell aging: do mitochondrial DNA mutations have a causal role? Aging Cell *13*, 201–205.

Banning, A., Deubel, S., Kluth, D., Zhou, Z., and Brigelius-Flohé, R. (2005). The GI-GPx gene is a target for Nrf2. Mol. Cell. Biol. *25*, 4914–4923.

Ben-David, U., and Benvenisty, N. (2011). The tumorigenicity of human embryonic and induced pluripotent stem cells. Nat. Rev. Cancer *11*, 268–277.

Boivin, A., Hanot, M., Malesys, C., Maalouf, M., Rousson, R., Rodriguez-Lafrasse, C., and Ardail, D. (2011). Transient alteration of cellular redox buffering before irradiation triggers apoptosis in head and neck carcinoma stem and non-stem cells. PLoS ONE *6*, e14558.

Brigelius-Flohé, R., and Kipp, A.P. (2012). Physiological functions of GPx2 and its role in inflammation-triggered carcinogenesis. Ann. N Y Acad. Sci. *1259*, 19–25.

Cervantes, R.B., Stringer, J.R., Shao, C., Tischfield, J.A., and Stambrook, P.J. (2002). Embryonic stem cells and somatic cells differ in mutation frequency and type. Proc. Natl. Acad. Sci. USA *99*, 3586–3590.

Dumitru, R., Gama, V., Fagan, B.M., Bower, J.J., Swahari, V., Pevny, L.H., and Deshmukh, M. (2012). Human embryonic stem cells have constitutively active Bax at the Golgi and are primed to undergo rapid apoptosis. Mol. Cell *46*, 573–583.

Facucho-Oliveira, J.M., Alderson, J., Spikings, E.C., Egginton, S., and St John, J.C. (2007). Mitochondrial DNA replication during differentiation of murine embryonic stem cells. J. Cell Sci. *120*, 4025–4034.

Filion, T.M., Qiao, M., Ghule, P.N., Mandeville, M., van Wijnen, A.J., Stein, J.L., Lian, J.B., Altieri, D.C., and Stein, G.S. (2009). Survival responses of human embryonic stem cells to DNA damage. J. Cell. Physiol. *220*, 586–592.

Ghoreschi, K., Brück, J., Kellerer, C., Deng, C., Peng, H., Rothfuss, O., Hussain, R.Z., Gocke, A.R., Respa, A., Glocova, I., et al. (2011). Fumarates improve psoriasis and multiple sclerosis by inducing type II dendritic cells. J. Exp. Med. *208*, 2291–2303.

Ginestier, C., Hur, M.H., Charafe-Jauffret, E., Monville, F., Dutcher, J., Brown, M., Jacquemier, J., Viens, P., Kleer, C.G., Liu, S., et al. (2007). ALDH1 is a marker of normal and malignant human mammary stem cells and a predictor of poor clinical outcome. Cell Stem Cell *1*, 555–567.

Jang, J., Wang, Y., Kim, H.S., Lalli, M.A., and Kosik, K.S. (2014). Nrf2, a regulator of the proteasome, controls self-renewal and pluripotency in human embryonic stem cells. Stem Cells *32*, 2616–2625.

Kipp, A.P., Müller, M.F., Göken, E.M., Deubel, S., and Brigelius-Flohé, R. (2012). The selenoproteins GPx2, TrxR2 and TrxR3 are regulated by Wnt signalling in the intestinal epithelium. Biochim. Biophys. Acta *1820*, 1588–1596.

Lehle, S., Hildebrand, D.G., Merz, B., Malak, P.N., Becker, M.S., Schmezer, P., Essmann, F., Schulze-Osthoff, K., and Rothfuss, O. (2014). LORD-Q: a long-run real-time PCR-based DNA-damage quantification method for nuclear and mitochondrial genome analysis. Nucleic Acids Res. *42*, e41.

Liu, J.C., Guan, X., Ryan, J.A., Rivera, A.G., Mock, C., Agrawal, V., Letai, A., Lerou, P.H., and Lahav, G. (2013). High mitochondrial priming sensitizes hESCs to DNA-damage-induced apoptosis. Cell Stem Cell *13*, 483–491.

Liu, J.C., Lerou, P.H., and Lahav, G. (2014). Stem cells: balancing resistance and sensitivity to DNA damage. Trends Cell Biol. *24*, 268–274.

Livak, K.J., and Schmittgen, T.D. (2001). Analysis of relative gene expression data using real-time quantitative PCR and the 2(-Delta Delta C(T)) method. Methods *25*, 402–408.

Ma, Y., Jin, J., Dong, C., Cheng, E.C., Lin, H., Huang, Y., and Qiu, C. (2010). High-efficiency siRNA-based gene knockdown in human embryonic stem cells. RNA *16*, 2564–2569.

Madden, D.T., Davila-Kruger, D., Melov, S., and Bredesen, D.E. (2011). Human embryonic stem cells express elevated levels of multiple pro-apoptotic BCL-2 family members. PLoS ONE *6*, e28530.

Maynard, S., Swistowska, A.M., Lee, J.W., Liu, Y., Liu, S.T., Da Cruz, A.B., Rao, M., de Souza-Pinto, N.C., Zeng, X., and Bohr, V.A. (2008). Human embryonic stem cells have enhanced repair of multiple forms of DNA damage. Stem Cells *26*, 2266–2274.

Momcilović, O., Choi, S., Varum, S., Bakkenist, C., Schatten, G., and Navara, C. (2009). Ionizing radiation induces ataxia telangiectasia mutated-dependent checkpoint signaling and G(2) but not G(1) cell cycle arrest in pluripotent human embryonic stem cells. Stem Cells *27*, 1822–1835.

Momcilović, O., Knobloch, L., Fornsaglio, J., Varum, S., Easley, C., and Schatten, G. (2010). DNA damage responses in human induced pluripotent stem cells and embryonic stem cells. PLoS ONE *5*, e13410.

Noh, K.H., Kim, B.W., Song, K.H., Cho, H., Lee, Y.H., Kim, J.H., Chung, J.Y., Kim, J.H., Hewitt, S.M., Seong, S.Y., et al. (2012). Nanog signaling in cancer promotes stem-like phenotype and immune evasion. J. Clin. Invest. *122*, 4077–4093.

Ohgushi, M., Matsumura, M., Eiraku, M., Murakami, K., Aramaki, T., Nishiyama, A., Muguruma, K., Nakano, T., Suga, H., Ueno, M., et al. (2010). Molecular pathway and cell state responsible for dissociation-induced apoptosis in human pluripotent stem cells. Cell Stem Cell *7*, 225–239.

Okita, K., and Yamanaka, S. (2011). Induced pluripotent stem cells: opportunities and challenges. Philos. Trans. R. Soc. Lond. B Biol. Sci. *366*, 2198–2207.

Park, I.H., Zhao, R., West, J.A., Yabuuchi, A., Huo, H., Ince, T.A., Lerou, P.H., Lensch, M.W., and Daley, G.Q. (2008). Reprogramming of human somatic cells to pluripotency with defined factors. Nature *451*, 141–146.

Prigione, A., Fauler, B., Lurz, R., Lehrach, H., and Adjaye, J. (2010). The senescence-related mitochondrial/oxidative stress pathway is repressed in human induced pluripotent stem cells. Stem Cells *28*, 721–733.

Qin, H., Yu, T., Qing, T., Liu, Y., Zhao, Y., Cai, J., Li, J., Song, Z., Qu, X., Zhou, P., et al. (2007). Regulation of apoptosis and differentiation by p53 in human embryonic stem cells. J. Biol. Chem. *282*, 5842–5852.

Robinton, D.A., and Daley, G.Q. (2012). The promise of induced pluripotent stem cells in research and therapy. Nature *481*, 295–305.

Roos, W.P., Christmann, M., Fraser, S.T., and Kaina, B. (2007). Mouse embryonic stem cells are hypersensitive to apoptosis triggered by the DNA damage O(6)-methylguanine due to high E2F1 regulated mismatch repair. Cell Death Differ. *14*, 1422–1432.

Saretzki, G., Walter, T., Atkinson, S., Passos, J.F., Bareth, B., Keith, W.N., Stewart, R., Hoare, S., Stojkovic, M., Armstrong, L., et al. (2008). Downregulation of multiple stress defense mechanisms during differentiation of human embryonic stem cells. Stem Cells *26*, 455–464.

Schieber, M., and Chandel, N.S. (2014). ROS function in redox signaling and oxidative stress. Curr. Biol. *24*, R453–R462.

St John, J.C., Amaral, A., Bowles, E., Oliveira, J.F., Lloyd, R., Freitas, M., Gray, H.L., Navara, C.S., Oliveira, G., Schatten, G.P., et al. (2006). The analysis of mitochondria and mitochondrial DNA in human embryonic stem cells. Methods Mol. Biol. *331*, 347–374.

Takahashi, K., Tanabe, K., Ohnuki, M., Narita, M., Ichisaka, T., Tomoda, K., and Yamanaka, S. (2007). Induction of pluripotent stem cells from adult human fibroblasts by defined factors. Cell *131*, 861–872.

Tapia, N., and Schöler, H.R. (2010). p53 connects tumorigenesis and reprogramming to pluripotency. J. Exp. Med. *207*, 2045–2048.

Tietze, F. (1969). Enzymic method for quantitative determination of nanogram amounts of total and oxidized glutathione: applications to mammalian blood and other tissues. Anal. Biochem. *27*, 502–522.

Yan, W., and Chen, X. (2006). GPX2, a direct target of p63, inhibits oxidative stress-induced apoptosis in a p53-dependent manner. J. Biol. Chem. *281*, 7856–7862.

Yu, J., Vodyanik, M.A., Smuga-Otto, K., Antosiewicz-Bourget, J., Frane, J.L., Tian, S., Nie, J., Jonsdottir, G.A., Ruotti, V., Stewart, R., et al. (2007). Induced pluripotent stem cell lines derived from human somatic cells. Science *318*, 1917–1920.

Stem Cell Reports, Volume *4*

Supplemental Information

High Glutathione and Glutathione Peroxidase-2 Levels Mediate Cell-Type-Specific DNA Damage Protection in Human Induced Pluripotent Stem Cells

Benjamin Dannenmann, Simon Lehle, Dominic G. Hildebrand, Ayline Kübler, Paula Grondona, Vera Schmid, Katharina Holzer, Mirjam Fröschl, Frank Essmann, Oliver Rothfuss, and Klaus Schulze-Osthoff

Supplementary Figures

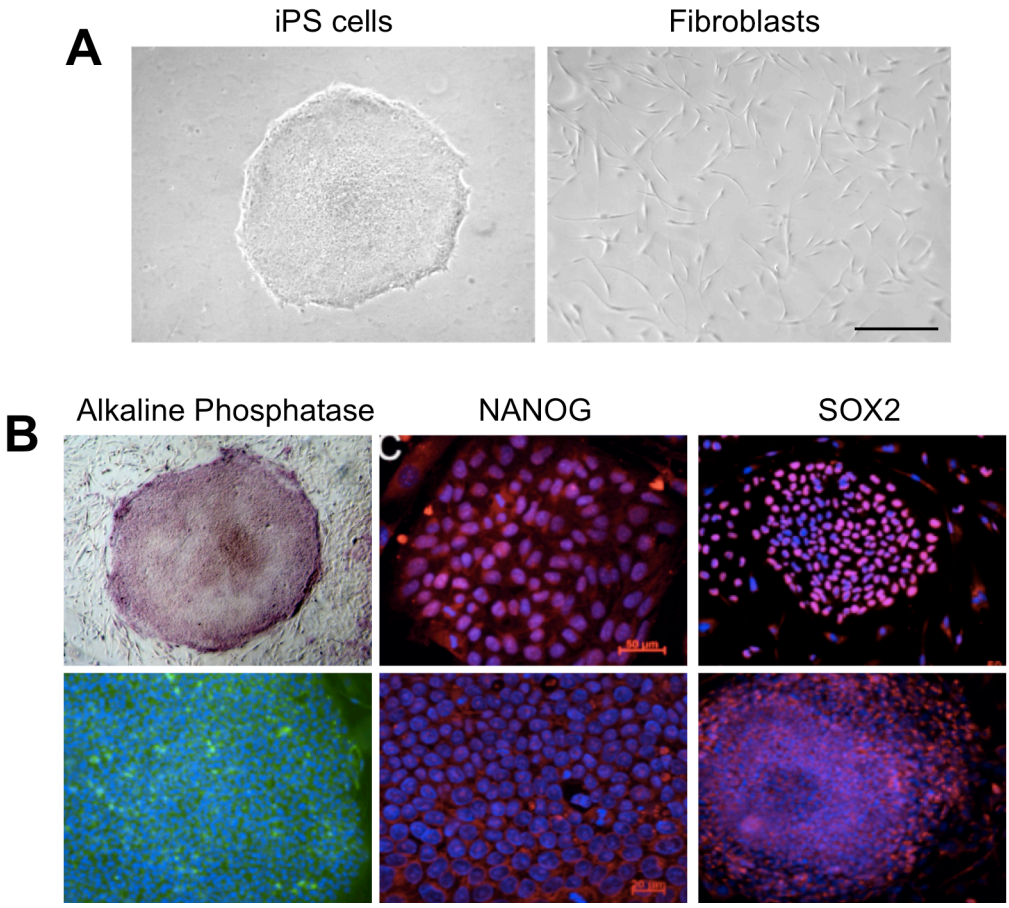

Figure S1: Characterization of employed human iPS cells and fibroblasts.

(A) Microscopical images of human dermal fibroblasts and iPS cells that were generated by retroviral transduction with *OCT4*, *SOX2*, *KLF4* and *c-MYC*. Scale bar = 200 µM.

(B) Alkaline phosphatase staining and expression of pluripotency markers NANOG, SOX2, TRA1-60, TRA1-81, and SSEA-4. Nuclei were visualized by blue DAPI staining. Exemplarily, L2 iPS cells (P25) and fibroblasts (P7) are shown.

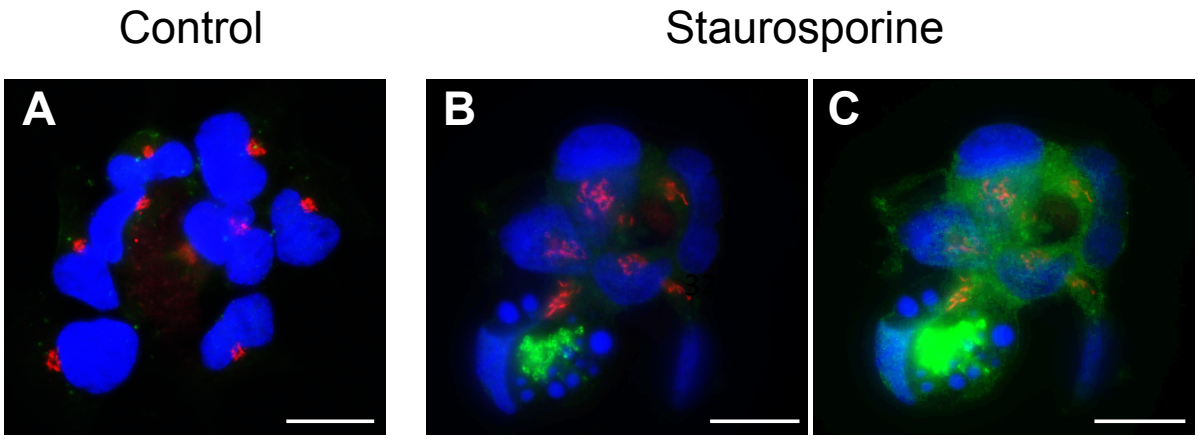

Figure S2: Human iPS cells do not maintain a constitutively active form of BAX at the Golgi.

Human iPS (iPSC L1) cells were either left untreated (A) or stimulated with 100 nM staurosporine (B, C) for 2 h to undergo apoptosis. Immunohistochemistry reveals that active Bax (green staining) is hardly detectable in healthy untreated cells and not present at the Golgi (red staining). An apoptotic cell shown in (B) reveals typical BAX clustering and nuclear fragmentation (blue staining). A brighter illumination of the picture (C) shows in pre-apoptotic cells an even cytosolic distribution of BAX but no localization at the Golgi. Scale bar = 20 µM. For indirect immunofluorescence cells were fixed in 4% formaldehyde and permeabilized in immunofluorescence buffer (PBS, 4% BSA, 0.05% saponin) for 1 h followed by over-night incubation at 4°C with conformation-specific anti-BAX-NT and the Golgi marker anti-GM130. Subsequently cells were washed and secondary antibodies were applied for 3 h at RT. Nuclei were stained for 5 min in PBS containing DAPI (10 ng/mL).

Supplementary Tables

Table S1: List of primary antibodies.

Specificity	Origin	Provider	Cat #/Address
Actin	Mouse	Sigma	A2228
Anti-mouse Alexa Fluor 488	Chicken	Invitrogen	A-21200
Anti-mouse Alexa Fluor 568	Rabbit	Invitrogen	A-11061
Anti-mouse Alexa Fluor 647	Chicken	Invitrogen	A-21463
Anti-rabbit Alexa Fluor 594	Chicken	Invitrogen	A-21442
Anti-rat Alexa Fluor 488	Chicken	Invitrogen	A-21470
BAD	Mouse	BD Transduction Laboratories	610391
BAK	Rabbit	Millipore (Upstate)	06-536
BAX	Mouse	Trevigen	2281-MC
BAX-NT (active BAX)	Rabbit	Millipore (Upstate)	06-499
BCL-2	Mouse	Santa Cruz	sc-7382
Bcl-X	Rabbit	BD	610212
BID	Goat	R&D	AF860
BIM	Rabbit	Stressgen	ADI-AAP-330-E
GM130	Rabbit	Abcam	EP892Y
GPX2	Rabbit	Anna P. Kipp	DIFE, Postdam-Rehbrücke, Germany
GSTA2	Rabbit	John Hayes	University of Dundee, UK
MCL-1	Mouse	BD Pharmingen	559027
NANOG	Rabbit	Abcam	ab21624
p53	Mouse	Calbiochem	OP43
Sox2	Rabbit	Abcam	ab59776
SSEA-4	Rat	Chemicon	MAB4303
TRA1-60	Mouse	Chemicon	MAB4360
TRA1-81	Mouse	Chemicon	MAB4381

Table S2: LORD-Q primers applied in DNA damage quantification experiments.

Locus	Base pairs	Efficiency	Primer Denotation	Primer Sequence
mtDNA (L)	3724	1.643	CL5.F	5'-ATCGTAGCCTTCTCCACTTC-3'
			AS2.R	5'-TGGTTAGGCTGGTGTTAGGG-3'
mtDNA (S)	50	1.989	AS2.F	5'-GGCCACAGCACTTAAACACA-3'
			AS2.R	5'-TGGTTAGGCTGGTGTTAGGG-3'
nDNA: *GAPDH* (L)	3653	1.660	*GAPDH*.F (1598)	5'-AGTCCCCAGAAACAGGAGGT-3'
			GAPDH.R (5250)	5'-GGCTGAGCTCCACTAACCAG-3'
nDNA: *GAPDH* (S)	45	1.995	*GAPDH*.F (4076)	5'-GCCTCACTCCTTTTGCAGAC-3'
			GAPDH.R (4128)	5'-GTCTTCTGGGTGGCAGTGAT-3'
nDNA: *TP53* (L)	3075	1.649	*TP53*.F	5'-CATAACCGCAAATGGGAAAC-3'
			TP53.R (3075)	5'-CGGGACGTGAAAGGTTAGAA-3'
nDNA: *TP53* (S)	45	1.991	*TP53*.F	5'-CATAACCGCAAATGGGAAAC-3'
			TP53.R (45)	5'-CGTCCTTTTGATGGCCTTT-3'

Table S3: Primers used in qRT-PCR experiments.

ACTB.F	5'-CATGTACGTTGCTATCCAGGC-3'
ACTB.R	5'-CTCCTTAATGTCACGCACGAT-3'
ALAS1.F	5'-CGCCGCTGCCCATTCTTAT-3'
ALAS1.R	5'-TCTGTTGGACCTTGGCCTTAG-3'
CAT.F	5'-TGTTGCTGGAGAATCGGGTTC-3'
CAT.R	5'-TCCCAGTTACCATCTTCTGTGTA-3'
GAPDH.F	5'-GGAGCGAGATCCCTCCAAAAT-3'
GAPDH.R	5'-GGCTGTTGTCATACTTCTCATGG-3'
GCLC.F	5'-GGAGGAAACCAAGCGCCAT-3'
GCLC.R	5'-CTTGACGGCGTGGTAGATGT-3'
GCLM.F	5'-TGTCTTGGAATGCACTGTATCTC-3'
GCLM.R	5'-CCCAGTAAGGCTGTAAATGCTC-3'
GDF3.F	5'-GCCATCAAAGAAAGGGAACA-3'
GDF3.R	5'-TCTGGCACAGGTGTCTTCAG-3'
GPX1.F	5'-CAGTCGGTGTATGCCTTCTCG-3'
GPX1.R	5'-GAGGGACGCCACATTCTCG-3'
GPX2.F	5'-GGTAGATTTCAATACGTTCCGGG-3'
GPX2.R	5'-TGACAGTTCTCCTGATGTCCAAA-3'
GPX3.F	5'-AGAGCCGGGGACAAGAGAA-3'
GPX3.R	5'-ATTTGCCAGCATACTGCTTGA-3'
GPX4.F	5'-GAGGCAAGACCGAAGTAAACTAC-3'
GPX4.R	5'-CCGAACTGGTTACACGGGAA-3'
GPX7.F	5'-CCCACCACTTTAACGTGCTC-3'
GPX7.R	5'-GGCAAAGCTCTCAATCTCCTT-3'
GSR.F	5'-TTCCAGAATACCAACGTCAAAGG-3'
GSR.R	5'-GTTTTCGGCCAGCAGCTATTG-3'
GSTA1.F	5'-CTGCCCGTATGTCCACCTG-3'
GSTA1.R	5'-AGCTCCTCGACGTAGTAGAGA-3'
GSTA2.F	5'-TACTCCAATATACGGGGCAGAA-3'
GSTA2.R	5'-TCCTCAGGTTGACTAAAGGGC-3'
GSTA4.F	5'-CCGGATGGAGTCCGTGAGAT-3'
GSTA4.R	5'-GGGCACTTGTTGGAACAGC-3'
GSTM1.F	5'-TCTGCCCTACTTGATTGATGGG-3'
GSTM1.R	5'-TCCACACGAATCTTCTCCTCT-3'
GSTM2.F	5'-TGTGCGGGGAATCAGAAAAGG-3'
GSTM2.R	5'-CTGGGTCATAGCAGAGTTTGG-3'
GSTM3.F	5'-TCGTGCGAGTCGTCTATGGT-3'
GSTM3.R	5'-TCTCCTCATAAGAGGTATCCGTG-3'
GSTM4.F	5'-AGAGGAGAAGATTCGTGTGGA-3'
GSTM4.R	5'-TGCTGCATCATTGTAGGAAGTT-3'
GSTM5.F	5'-CCATCCTGCGCTACATTGC-3'
GSTM5.R	5'-CCAGCTCCATGTGGTTATCCAT-3'
GSTO1.F	5'-GAACGGCTGGAAGCAATGAAG-3'
GSTO1.R	5'-TGCCATCCACAGTTTCAGTTT-3'

GSTO2.F	5'-TGCCCCTATTCTCACAGGACC-3'
GSTO2.R	5'-TCCAGGTACTCACAAGCAATAAC-3'
GSTT1.F	5'-TGCCGCGCTGTTTACATCTT-3'
GSTT1.R	5'-GTGCTGACCTTTAATCAGATCCA-3'
GSTT2.F	5'-TGGCATCCCCTTAGAGCTG-3'
GSTT2.R	5'-CTTGAGCGTCGGCAGTTTC-3'
GSTZ1.F	5'-GCCCAGAACGCCATCACTT-3'
GSTZ1.R	5'-CTACACAGTATATGCCCGCTG-3'
MGST1.F	5'-ATGACAGAGTAGAACGTGTACGC-3'
MGST1.R	5'-TACAGGAGGCCAATTCCAAGA-3'
MGST2.F	5'-TCGGCCTGTCAGCAAAGTTAT-3'
MGST2.R	5'-TGCCCGAAATACTCTCTCAAAC-3'
MGST3.F	5'-GGCCCACCTAGCCATCAATG-3'
MGST3.R	5'-CGCTGAATGCAGTTGAAGATGT-3'
NANOG.F	5’-ACTCTCCAACATCCTGAACCTC-3’
NANOG.R	5’-GCCTTCTGCGTCACACCA-3’
PRDX1.F	5'-CATTCCTTTGGTATCAGACCCG-3'
PRDX1.R	5'-CCCTGAACGAGATGCCTTCAT-3'
PRDX2.F	5'-GAAGCTGTCGGACTACAAAGG-3'
PRDX2.R	5'-TCGGTGGGGCACACAAAAG-3'
PRDX3.F	5'-GAGACTACGGTGTGCTGTTAGA-3'
PRDX3.R	5'-GTTGACGCTCAAATGCTTGATG-3'
PRDX4.F	5'-AGAGGAGTGCCACTTCTACG-3'
PRDX4.R	5'-GGAAATCTTCGCTTTGCTTAGGT-3'
PRDX6.F	5'-GTTGCCACCCCAGTTGATTG-3'
PRDX6.R	5'-TGAAGACTCCTTTCGGGAAAAGT-3'
SOD1.F	5'-GGTGGGCCAAAGGATGAAGAG-3'
SOD1.R	5'-CCACAAGCCAAACGACTTCC-3'
SOD2.F	5'-GCTCCGGTTTTGGGGTATCTG-3'
SOD2.R	5'-GCGTTGATGTGAGGTTCCAG-3'
SOD3.F	5'-ATGCTGGCGCTACTGTGTTC-3'
SOD3.R	5'-CTCCGCCGAGTCAGAGTTG-3'
TMX1.F	5'-AGTATGTCAGCACTCTTTCAGC-3'
TMX1.R	5'-CACACTGGCAATCCAAGGTCT-3'
TXN.F	5'-GTGAAGCAGATCGAGAGCAAG-3'
TXN.R	5'-CGTGGCTGAGAAGTCAACTACTA-3'
TXNIP.F	5'-GGTCTTTAACGACCCTGAAAAGG-3'
TXNIP.R	5'-ACACGAGTAACTTCACACACCT-3'